Influence of Magnesium Source on the Mechanochemical Synthesis of Magnesium-Substituted Hydroxyapatite

Natalia V. Bulina *, Nataly V. Eremina, Svetlana V. Makarova, Irina A. Borodulina, Olga B. Vinokurova, Leon A. Avakyan, Ekaterina V. Paramonova, Vladimir S. Bystrov, Olga A. Logutenko

Posted Date: 7 December 2023

doi: 10.20944/preprints202312.0442.v1

Keywords: hydroxyapatite; substitution; doping; magnesium; synthesis; mechanochemistry; thermal stability; density functional theory

Article

Influence of Magnesium Source on the Mechanochemical Synthesis of Magnesium-Substituted Hydroxyapatite

Natalia V. Bulina [1,*], Nataly V. Eremina [1], Svetlana V. Makarova [1], Irina A. Borodulina [1], Olga B. Vinokurova [1], Leon A. Avakyan [2], Ekaterina V. Paramonova [3], Vladimir S. Bystrov [3] and Olga A. Logutenko [1]

[1] Institute of Solid State Chemistry and Mechanochemistry, Siberian Branch of the Russian Academy of Sciences, Kutateladze Str. 18, 630090 Novosibirsk, Russia; bulina@solid.nsc.ru (B.N.V.); eremina@solid.nsc.ru (N.V.E.); makarova@solid.nsc.ru (S.V.M.); ir.an.bor@yandex.ru (I.A.B.); sveta070796@mail.ru (O.B.V.); olga_logutenko@mail.ru (O.A.L.)

[2] Physics Faculty, Southern Federal University, Rostov-on-Don 344090, Russia; laavakyan@sfdeu.ru (L.A.A.);

[3] Institute of Mathematical Problems of Biology - Branch of Keldysh Institute of Applied Mathematics, Russian Academy of Sciences, 142290 Pushchino, Russia; vsbys@mail.ru (V.S.B.); ekatp11@gmail.com (E.V.P.)

* Correspondence: bulina@solid.nsc.ru; Tel.: +7-383-233-24-10

Abstract: Magnesium, as one of the most abundant cation in the human body, plays an important role in both physiological and pathological processes. In this study, it was shown that a promising biomedical material Mg-substituted hydroxyapatite (Mg-HA) can be synthesized via fast mechanochemical method. For this method, the nature of magnesium-contained carriers was shown to be important. When using magnesium oxide as a source of magnesium, the partial insertion of magnesium cations into the apatite structure occurs. In contrast, when magnesium hydroxide or monomagnesium phosphate is used, a single-phase Mg-HA is formed. Both experimental and theoretical investigations showed that an increase in the Mg content leads to a decrease in the lattice parameters and unit cell volume of Mg-HA. Density functional theory calculations showed the high sensitivity of the lattice parameters towards the crystallographic position of the calcium site substituted by magnesium. It was shown experimentally that insertion of magnesium cations decreases the thermal stability of the hydroxyapatite. The thermal decomposition of Mg-HA leads to the formation of a mixture of stoichiometric HA, magnesium oxide and Mg-substituted tricalcium phosphate phases.

Keywords: hydroxyapatite; substitution; doping; magnesium; synthesis; mechanochemistry; thermal stability; density functional theory

1. Introduction

Hydroxyapatite (HA), $Ca_{10}(PO_4)_6(OH)_2$, is widely used as a drug carrier for targeted drug delivery in various fields of medicine including traumatology and orthopedics, craniofacial surgery and dental technology, therapy and cosmetology. HA has become a material for the preparation of biocompatible ceramic products, composites, bone defect fillers, medical cements and implants [1–3]. This wide medical application is due to its similarity to the minerals of human bone and dental tissue.

The HA unit cell contains ten calcium cations, six PO_4^{4-} tetrahedrons, and two hydroxyl groups located on the *c*-axis (Figure 1). The hydroxyl groups are surrounded by calcium cations forming through-channels in the HA crystal [4]. The stoichiometric HA has a Ca/P atomic ratio of 1.67. Its structure is remarkable since all ions in the HA structure can be substituted, and replacement with

Preprints (www.preprints.org) | NOT PEER-REVIEWED | Posted: 7 December 2023 doi:10.20944/preprints202312.0442.v1

both isovalent and heterovalent ions of other chemical elements or their chemical groups is possible [5,6].

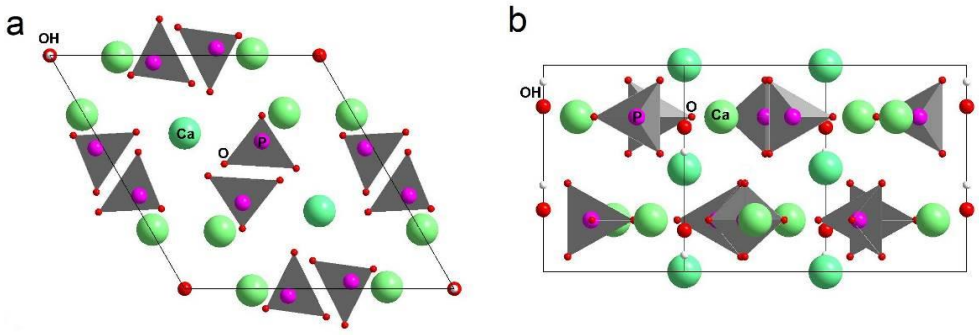

Figure 1. A view of the crystal structure of HA along the *c* axis (**a**) and the *b* axis (**b**).

Magnesium is the fourth most abundant cation in the human body after calcium, potassium and sodium [7]. Magnesium is present in various human organs and plays an important role in a variety of processes. Approximately 60% of the magnesium is located in bone tissue, which is almost 1% of the total bone mineral content [7]. Magnesium ion deficiency can directly affect the bone properties by altering the structure and size of bone crystals of the biogenic HA as it affects bone metabolism [8–10]. Also, magnesium cations are particularly important for bone density. Thus, some studies show that magnesium deficiency promotes osteoporosis, fragility, microfractures of the trabeculae [11–13] and the reduction of bone's mechanical properties [14,15]. Therefore, the substitution of calcium cations with magnesium cations in synthetic HA attracts huge attention [16–18].

The synthesis of magnesium-substituted HA (Mg-HA) is usually carried out by chemical precipitation from aqueous solution, which under certain conditions results in the formation of a single-phase product [13,16,17,19–25]. According to Shepherd et al. [26], Mg-HA has the composition $Ca_{10-x}Mg_x(PO_4)_6(OH)_2$. Ren et al. [19] reported that there is a limit of the magnesium content in HA of $x = 1.5$ when precipitation methods are used. Alternatively, the conventional hydrothermal methods [27,28] can be used to obtain single-phase Mg-HA with higher Mg content limit of $x = 3$ [25,27].

According to studies [11,23,25,27,29], the introduction of magnesium ions into the HA crystal lattice leads to a decrease of the cell parameters due to the significantly smaller radius of Mg^{2+} (0.65 Å) than Ca^{2+} (0.99 Å). However, Nagyné-Kovács et al. reported on the decrease of the unit cell parameter *a* and the increase of the parameter *c* [21], the increase of parameter *a* is also reported by Farzadi et al. [22]. In these studies the same method of Mg-HA synthesis was used, but with different reagents and synthesis stages. It is expected that the synthesis conditions have great significance and affect the composition of the as-synthesized HA.

Several studies showed that magnesium complicates the crystallization of apatite and destabilizes its structure, which promotes its thermal transformation to β-tricalcium phosphate (β-TCP) in the 700–900 °C temperature range [13,17,23,30–33]. In contrast there are studies reported that Mg-HA with low degree of substitution remains stable at temperatures higher than 900°C [11,17,20,21,29].

The aim of the present work is to explore the possibility of Mg-HAs preparation by simple mechanochemical method using different magnesium sources, and to study structure and thermal stability of the as-synthesized Mg-HAs.

2. Materials and Methods

2.1. Samples Preparation

The mechanochemical synthesis of Mg-HA samples with different concentration of substituent ions was carried out in a planetary ball mill AGO-2 (Russia) in steel drums with the 200 g steel balls at a rotation speed of 1800 rpm. Calcium hydroorthophosphate, $CaHPO_4$ (analytical grade, Vekton,

 doi:10.20944/preprints202312.0442.v1

Saint Petersburg, Russia), freshly calcined calcium oxide, CaO (analytical grade, Vekton, Saint Petersburg, Russia), magnesium oxide, MgO (pure grade, Vekton, Saint Petersburg, Russia), magnesium hydroxide, $Mg(OH)_2$ (analytical grade, Vekton, Saint Petersburg, Russia), and magnesium dihydrogen phosphate dehydrate, $Mg(H_2PO_4)_2{\cdot}2H_2O$ (analytical grade, Vekton, Saint Petersburg, Russia), were used as the initial reagents.

The initial reagents were mixed in ratios according to reactions (1–3), while calcium cations were replaced by magnesium cations keeping the (Ca+Mg)/P ratio constant at 1.67:

$$6CaHPO_4 + (4-x)CaO + x\,MgO \rightarrow Ca_{10-x}Mg_x(PO_4)_6(OH)_2 + 2H_2O \quad (1)$$

$$6CaHPO_4 + (4-x)CaO + x\,Mg(OH)_2 \rightarrow Ca_{10-x}Mg_x(PO_4)_6(OH)_2 + (2+x)H_2O \quad (2)$$

$$(6-2x)CaHPO_4 + (4+x)CaO + xMg(H_2PO_4)_2{\cdot}2H_2O \rightarrow Ca_{(10-x)}Mg_x(PO_4)_6(OH)_2 + (2+3x)\,H_2O \quad (3)$$

where x = 0, 0.25, 0.5, 1.0, 1.5, 2.0

The mechanochemical treatment of the reaction mixture was carried out for 30 min. The lining of the balls and the inner surface of the drums was carried out with the reaction mixture. According to atomic absorption analysis, the iron content in the samples after synthesis did not exceed 0.05 wt.%.

The thermal stability of the as-synthesized compounds was studied in a laboratory electrical furnace SNOL February 7, 1100 (Umega, Latvia) by heating in air at temperatures of 500, 600, 700, 800, 900, and 1100 °C for 2 h. The rate of heating and cooling was 5 °C/min.

2.2. Samples Characterization

Powder X-ray diffraction (XRD) patterns of the as-synthesized and heated samples were recorded on a D8 Advance powder diffractometer (Bruker, Mannheim, Germany) with Bragg-Brentano geometry using CuKα radiation in the range 2θ = 10°–70° using a step size of 0.02° and an accumulated time per step of 35 s. Phase identification was carried out using the PDF-4 database (ICDD, Release 2011). The unit cell parameters, crystallite size, and phase concentrations were determined by the Rietveld method [34] using Topas 4.2 software (Bruker, Mannheim, Germany). The fundamental parameter approach was used to account for the instrumental contribution.

Fourier transform infrared (FTIR) spectra of the powders were recorded on an Infralum FT-801 spectrometer (Simex, Russia) in the wavelength range 550–4000 cm^{-1}. Pellets made up of a 4 mg sample and 540 mg KBr were used for the FTIR study.

Thermal analysis experiments were carried out using a STA 449 F1 Jupiter device (Netzsch, Selb, Germany) equipped with a QMS 403C Aeolos mass spectrometer. The measurements were performed under an argon–oxygen mixture (80:20) at a heating rate of 10 °C/min. The analyzed sample with a mass of 30 mg was placed in a corundum crucible.

2.3. Computational Details

Atomic and electronic structure of HA was calculated within density functional approach as described in our study [35]. Concisely, the electronic band structure and formation energies were calculated using precise hybrid exchange-correlation functional (i.e. HSE06 [36,37] based on the geometries obtained using less precise semi-local functional (PBE [38]). The simulation cell is selected as a 2×2×2 orthorhombic supercell (352 atoms, as illustrated in Figure 2) which is sufficiently large to diminish the spurious interaction between defects in the neighboring cells.

Preprints (www.preprints.org) | NOT PEER-REVIEWED | Posted: 7 December 2023 doi:10.20944/preprints202312.0442.v1

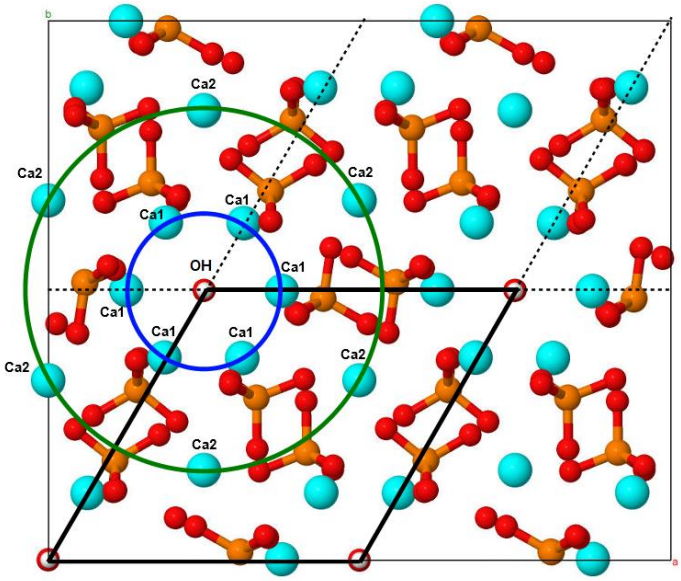

Figure 2. The illustration of the considered HA supercell containing 352 atoms, as viewed from the *c* axis. The bold black lines illustrate the hexagonal unit cell of HA (contains 44 atoms, fig. 1) in the considered orthorhombic supercell. Adapted from [35].

The computations were performed using the QUANTUM EPSRESSO software package [39], operating within the plane-wave formalism. We used norm-conserved pseudo-potentials to represent the core electron states, the basis set was limited by cut-off energy of 60 Ryd and of 120 Ryd for exchange correlation operator used in hybrid functional. The detailed information about selection of the calculation parameters is available in [35].

HA structure has two crystallographic positions of Ca cations (Figure 2) and both of them could be substituted by Mg cations. We considered structure models of both types of the substitutions with degree substitution x (count of substitutions per HA unit cell) varied from 0.1 to 2.0.

Previous studies [35] showed a decrease in the parameters and volume of the HA cell when calcium is substituted for magnesium in the Ca1 and Ca2 positions with the increase of magnesium concentration x, which is in agreement with the results of other authors [19, 40]. However, at higher concentrations (x ~ 2), the convergence of the calculation was not quite sufficient because of the more severe structural changes, which required more thorough calculations. In this work, we present the results of such calculations performed using of large scale computational facilities, which allowed to achieve the necessary predetermined criteria of ion relaxation in the Mg-HA structure and to improve the results presented in [35]. The structural optimization was continued till the difference between total energy at the last two steps remains higher than the predetermined threshold of 10^{-4} eV and the maximal force acting on atoms is above 0.01 eV/Å.

The formation energy E_f of calcium to magnesium substitution for different values of n (the number of magnesium ions in the supercell) was calculated by the formula [35]:

$$E_f = E_{tot} - E_{HA} - n\cdot[\mu(Mg) - \mu(Ca)], \quad (4)$$

where E_{HA} is the total energy of the original unsubstituted HA structure taken for a 2x2x2 = 8 supercell, which after full density functional theory (DFT) calculation with the HSE functional has the value E_{HA} = -180083.6377291 eV; E_{tot} is the total energy of the substituted HA-Mg, calculated after full relaxation of the supercell with a given number n of substitutions; μ(Mg) and μ(Ca) are the chemical potentials of Mg and Ca ions, calculated for the reference phases of *hcp* Mg and *fcc* Ca, correspondingly: μ(Mg) = -1478.734 eV and μ(Ca) = -1003.756 eV.

The E_f values obtained as a result of the calculation are normed per one formula unit (f.u.) of the HA unit cell.

Preprints (www.preprints.org) | NOT PEER-REVIEWED | Posted: 7 December 2023 doi:10.20944/preprints202312.0442.v1

3. Results and Discussion

3.1. Mechanochemical Synthesis of Mg-HA

Figure 3 shows the XRD patterns of the products prepared from different magnesium-based reagents according to reactions (1–3). As seen, all the XRD patterns of the samples produced from magnesium oxide have reflections of the initial MgO at 2θ = 43.03° and HA phases (Figure 3a). At x = 2 there is also a reflex at 2θ = 31.25°, which belongs to the β-$Ca_3(PO_4)_2$ (TCP) phase. The XRD patterns of the samples synthesized using $Mg(OH)_2$ and $Mg(H_2PO_4)_2{\cdot}2H_2O$ contain only the apatite phase reflections (Figure 3b,c). This leads to the conclusion that reactions 2 and 3 proceed entirely to completion, i.e. all the reagents participate in the formation of the Mg-HA structure, which is not the case for reaction 1. Table 1 shows that the concentration of MgO in the resultant products is about two times less than that introduced into the initial mixture. Therefore, only a part of magnesium oxide reacts with the other components to form Mg-HA by reaction 1.

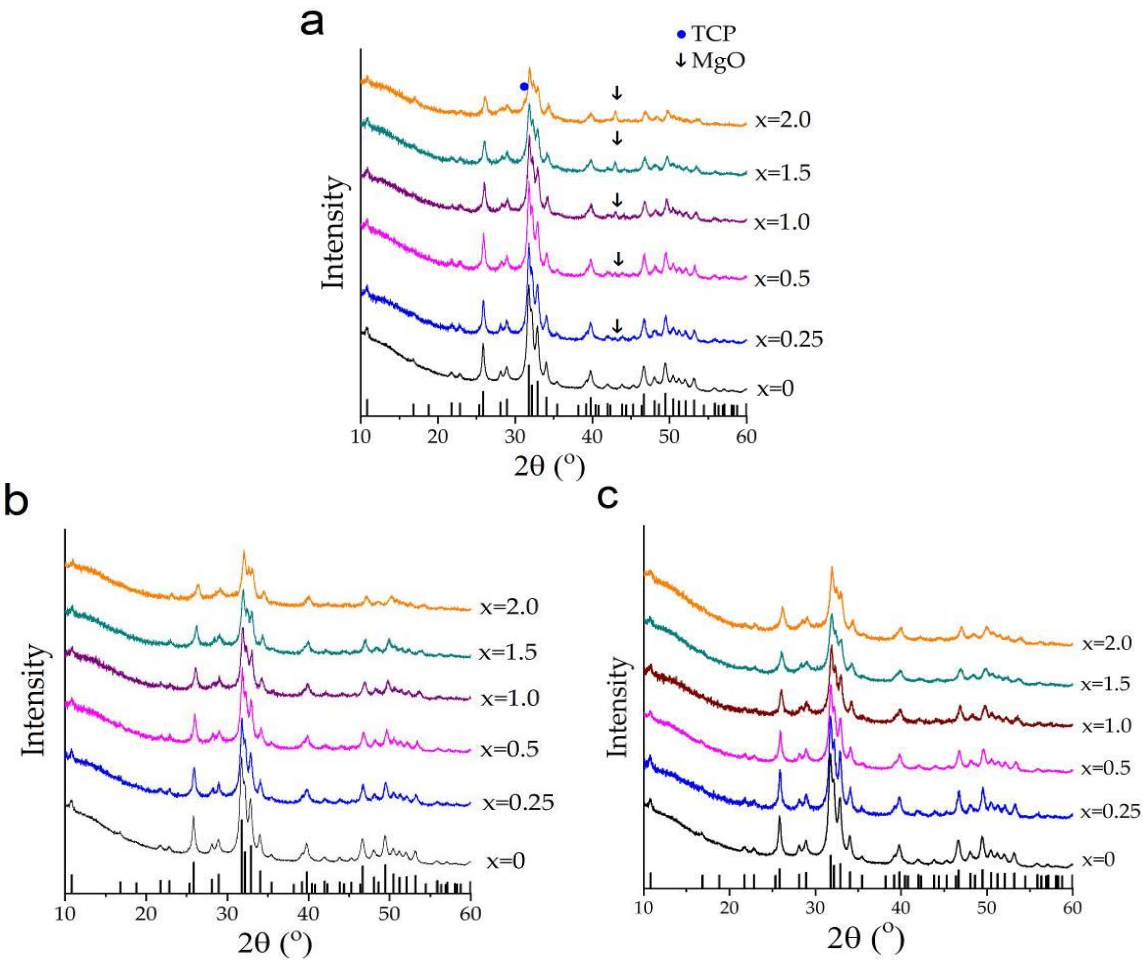

Figure 3. XRD patterns of the samples synthesized with different concentration of MgO (**a**), $Mg(OH)_2$ (**b**), and $Mg(H_2PO_4)_2{\cdot}2H_2O$ (**c**). Vertical bars in the (**a**) graph correspond to the HA phase from the ICDD database (PDF No. 40-11-9308).

Table 1. Results of the quantitative analysis of the samples produced using magnesium oxide.

Initial concentration		Powder composition after synthesis, wt.%		
x(Mg)	MgO, wt.%	Mg-HA	MgO	TCP
0	0	100	0	0
0.25	0.97	99.5	0.5	0
0.5	1.95	99.3	0.7	0
1.0	3.93	98.1	1.9	0

Preprints (www.preprints.org) | NOT PEER-REVIEWED | Posted: 7 December 2023 doi:10.20944/preprints202312.0442.v1

1.5	5.94	96.2	3.8	0
2.0	7.99	82.9	6.4	10.7

The changes in the cell and volume parameters in the substituted samples depending on the concentration of the introduced magnesium oxide confirm the presence of magnesium cations in the structure of the as-synthesized Mg-HA (Figure 4). As seen, the most significant decrease in these values is observed for the samples prepared by reaction 2, with magnesium hydroxide used as the Mg source. This can be attributed to the different ionic radii of calcium and magnesium cations: $R(Ca^{2+})$ = 1.00 Å, $R(Mg^{2+})$ = 0.72 Å [41]. In the case of MgO, a decrease in these parameters is not so marked because not all the magnesium has reacted, as mentioned above. In the case of monomagnesium phosphate, the larger changes in the parameters at large values of x, unlike the case of magnesium hydroxide, can be explained by the influence of a large number of water molecules released during the chemical interaction of this mixture of the reactants (reaction 3), which can increase the lattice parameter values. An interesting fact is that the concentration of the released water does not affect the crystallite size (Figure 4c). Although the dopant concentration affects it; thus, the larger *x*, the smaller the average crystallite size is.

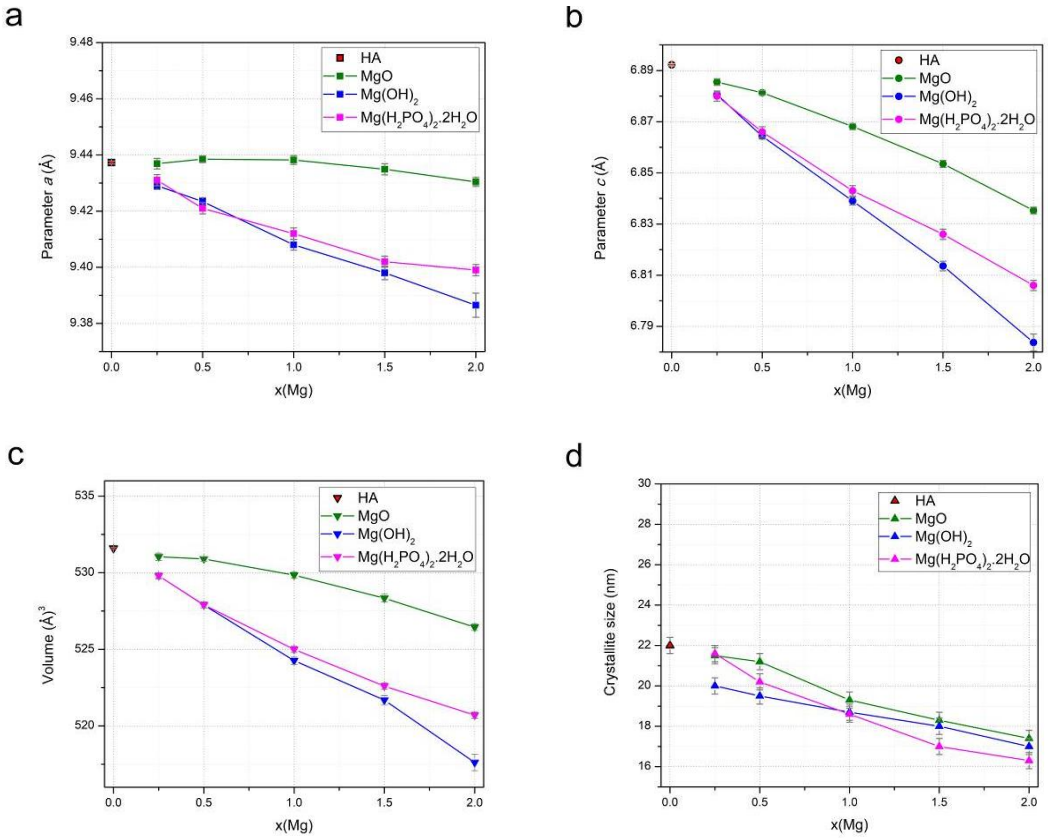

Figure 4. Variation of the parameters *a* (**a**) and *c* (**b**), unit cell volume (**c**) and crystallite size (**d**) of the Mg-HA phase in the as-synthesized samples as a function of magnesium concentration in the initial mixture when using different magnesium-based reagents.

The low reactivity of magnesium oxide in mechanochemical synthesis may be due to its high mechanical strength and strong abrasive resistance (periclase has a Mohs hardness value of 5.5, calcium oxide – 3.5), unlike the other reactants of the reaction mixture that are prone to hydration. The authors of study [42] reported that, in the first minutes of the mechanochemical treatment of the initial mixture in a planetary ball mill, the grinding of the reagents occurs followed by the neutralization reaction with the formation of HA crystallites. The different degree of grinding of the reagents, resulted from their different hardness, does not allow the particles to be efficiently distributed over the volume of the reaction mixture. Therefore, only a small part of the surface layer of MgO particles is involved in Reaction (1). In this case, magnesium-deficient apatite with low

Preprints (www.preprints.org) | NOT PEER-REVIEWED | Posted: 7 December 2023 doi:10.20944/preprints202312.0442.v1

(Ca+Mg)/P ratio (< 1.67) is formed. With a deficiency of calcium ions in the HA cationic sublattice, the so-called "acidic" apatite $Ca_{10-y}(HPO_4)_y(PO_4)_{6-y}(OH)_{2-y}$ is formed during mechanochemical synthesis [43]. In our case, since a part of magnesium can be incorporated into the apatite crystal structure, the possible composition of the as-synthesized apatite is $Ca_{10-x}Mg_{x-y}(HPO_4)_y(PO_4)_{6-y}(OH)_{2-y}$, where y < x. Consequently, reaction (1) can be re-written as follows:

$$6CaHPO_4 + (4-x)CaO + xMgO \rightarrow Ca_{10-x}Mg_{x-y}(HPO_4)_y(PO_4)_{6-y}(OH)_{2-y} + yMgO + 2H_2O \quad (5)$$

The presence of $(HPO_4)^{2-}$ groups in the structure of Mg-HA prepared from magnesium oxide is confirmed by the FTIR spectra (Figure 5), which show a corresponding absorption band at 880 cm^{-1} [43], which is not observed in the spectra of the samples synthesized using magnesium hydroxide (Figure 5b). The absorption bands of the phosphate anion (572, 602, 960, 1048, 1090 cm^{-1}) and the bands of stretching (3572 cm^{-1}) and libration (630 cm^{-1}) vibrations of the hydroxyl group in the HA structure appear in both spectra [4]. The broad bands at 1640 and 3430 cm^{-1} belong to adsorbed water, while the low-intensity bands at 1420 and 1470 cm^{-1} correspond to the low carbonate ion content [4].

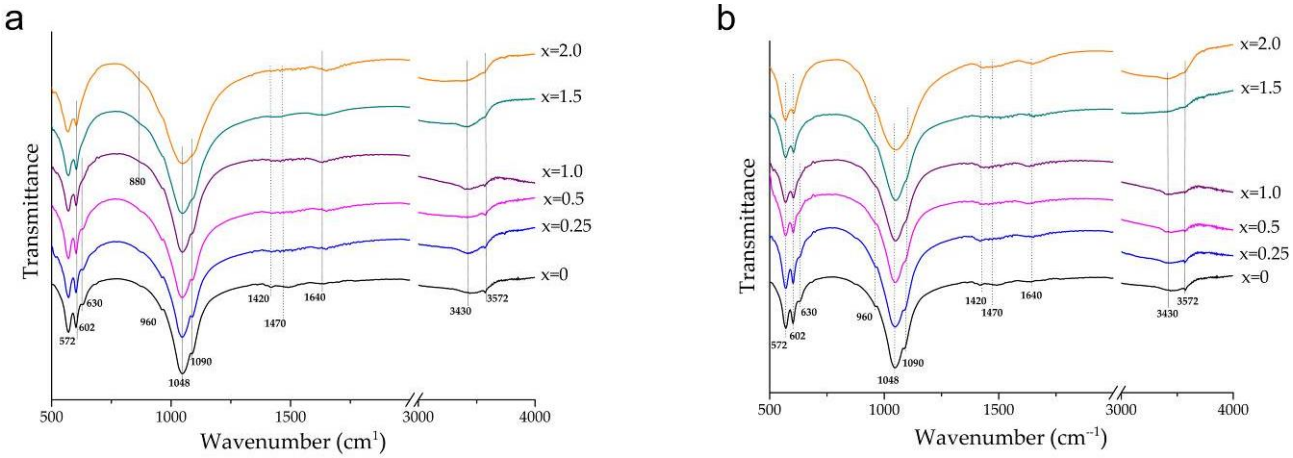

Figure 5. FTIR spectra of the samples synthesized with different concentration of MgO (**a**) and $Mg(H_2PO_4)_2{\cdot}2H_2O$ (**b**).

The STA data confirm the presence of adsorbed and lattice water in the synthesized samples, which is released in the temperature range of 50–600 °C (Figure 6). The amount of water in the samples is different and consistent with the stoichiometry of reaction equations (1)–(3). When MgO, $Mg(OH)_2$, and $Mg(H_2PO_4)_2{\cdot}2H_2O$ are used as the Mg sources, the amount of water released from the samples is 4.1, 7.1, and 7.2 wt.% respectively. The endoeffects observed in the DTA curves at higher temperatures are obviously related to the decomposition of the substituted apatite structure.

Preprints (www.preprints.org) | NOT PEER-REVIEWED | Posted: 7 December 2023 doi:10.20944/preprints202312.0442.v1

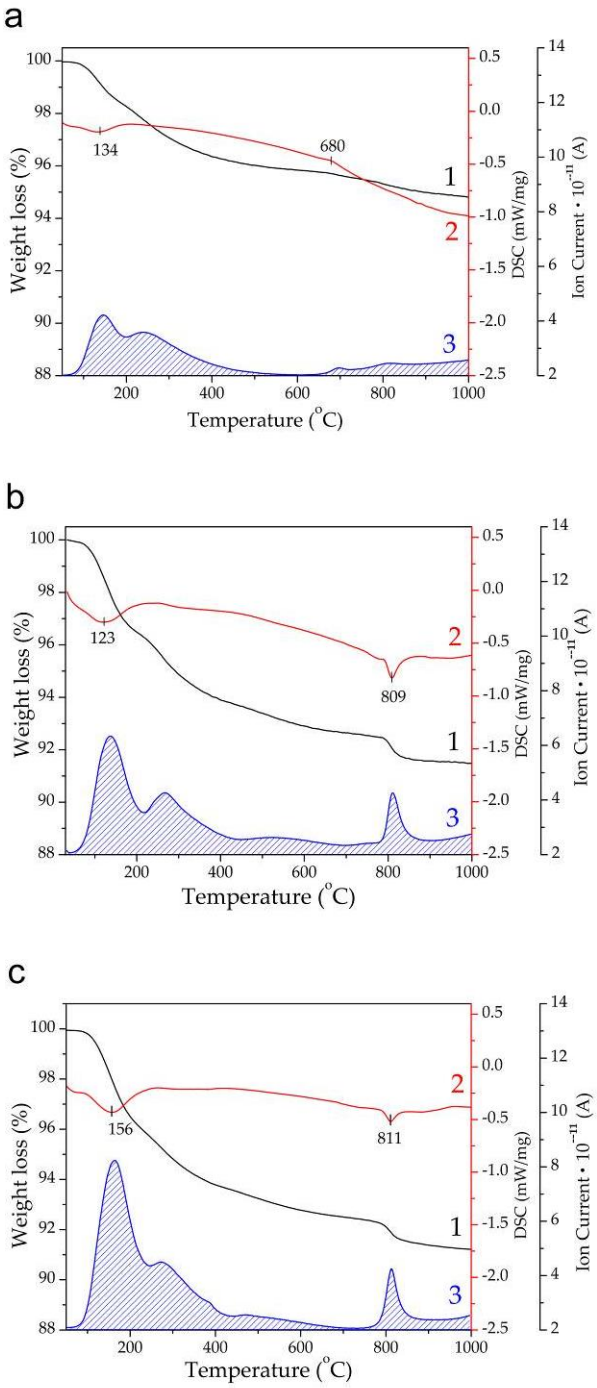

Figure 6. STA of the Mg–HA samples synthesized using MgO (**a**), $Mg(OH)_2$ (**b**) and $Mg(H_2PO_4)_2 \cdot 2H_2O$ (**c**): 1 – weight loss; 2 – DSC; 3 – water release.

The data shown in Table 2 indicate that the removal of adsorbed water does not change the phase composition of the samples synthesized with the addition of magnesium hydroxide and monomagnesium phosphate. They remain single phase in contrast to the samples synthesized with the incorporation of magnesium oxide. Heating of the samples obtained with MgO led to an increase in the MgO concentration and the formation of the TCP phase at $x = 1.5$.

Preprints (www.preprints.org) | NOT PEER-REVIEWED | Posted: 7 December 2023 doi:10.20944/preprints202312.0442.v1

Table 2. Phase composition (wt.%) of the synthesized samples with different *x* after heating at 500 °C.

Initial concentration of Mg (*x*)	MgO using (reaction *1*)			$Mg(OH)_2$ using (reaction *2*)	$Mg(H_2PO_4)_2{\cdot}2H_2O$ using (reaction *3*)
	Mg-HA	MgO	TCP	Mg-HA	Mg-HA
0	100	0	0	100	100
0.25	99.2	0.8	0	100	100
0.5	98.6	1.4	0	100	100
1.0	97.5	2.5	0	100	100
1.5	92.6	3.3	4.1	100	100
2.0	74.8	4.1	21.1	100	100

Figure 7 shows the changes in the unit cell parameters of the Mg-HA phase in the samples after heating at 500 °C. Comparing the data shown in this figure with those shown in Figure 4, it is evident that, after heating, the parameters keep changing with increasing *x* but not that much. At the same time, after the removal of water, the lattice parameters and cell volumes of the samples synthesized using $Mg(OH)_2$ and $Mg(H_2PO_4)_2{\cdot}2H_2O$ are nearly the same and keep decreasing with increasing *x*. This suggests that the samples with the same *x* are of comparable magnesium concentrations in the Mg-HA lattice. As for the samples synthesized using magnesium oxide, the change in the parameter *c* is very similar to that for the samples obtained using both $Mg(OH)_2$ and $Mg(H_2PO_4)_2{\cdot}2H_2O$, although the parameter *a* increases with an increase in *x*. The different trend in changing the parameter *a* for the samples obtained with MgO may be caused by an increase in the number of vacancies of the OH groups in the Mg-HA structure [4] in accordance with Formula (4). The decrease of the parameter *c* in this case is due to the increase in the number of substitutions of the calcium positions with both the magnesium and hydrogen ion of the group $(HPO_4)^{2-}$, located also in the region of the vacant position of the calcium cation. After the water has been removed from the Mg-HA samples, the crystallite size of the apatite phase gradually decreases with increasing *x* for all series of samples (Figure 7d).

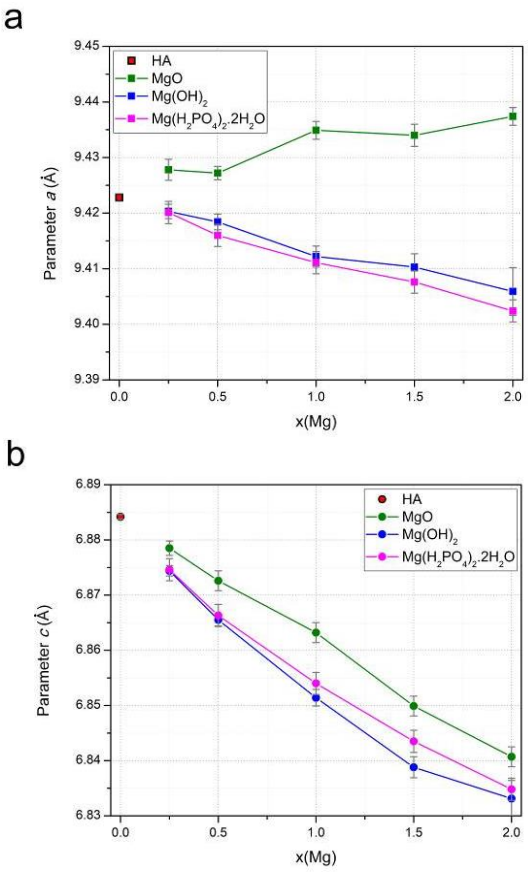

Preprints (www.preprints.org) | NOT PEER-REVIEWED | Posted: 7 December 2023 doi:10.20944/preprints202312.0442.v1

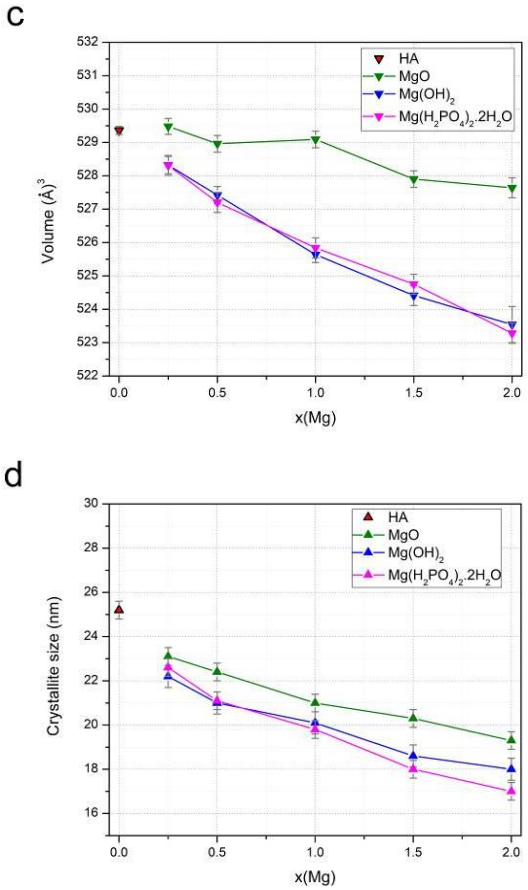

Figure 7. Changes in the parameters *a* (**a**) and *c* (**b**), unit cell volume (**c**) and crystallite size (**d**) of Mg-HA phase in the annealed at 500 °C samples depending on the magnesium concentration in the initial mixture when using different magnesium-based reagents.

3.2. Lattice Parameters Predicted by DFT

The purpose of this section is to provide a theoretical insight on the incorporation of Mg^{2+} in the HA crystal lattice, since it is not possible to refine experimentally the structure of the substituted apatite in this case due to its small crystallite size and the low electron density of the substituent cation.

Figure 8 shows the calculated cell parameters for models containing different amount of Ca1 and Ca2 substitutions. As can be seen, the general tendency is the decrease of the unit cell size with the addition of Mg cations. However, the differences of the positions of the substituted Ca cations have significant effect on the cell parameters at high x. In particular, at $x > 1$, the cell parameters a and b decrease noticeably if magnesium is located in the Ca1 position, while the parameter c increases only slightly. In the case of the Ca2 substitutions all parameters decreases but slower, than in the case of Ca1, so that the unit cell volumes at the same x in both substitutions have comparable values in the whole range of magnesium concentrations and they decrease almost linearly with the increasing of the number of substitutions in the cell.

Preprints (www.preprints.org) | NOT PEER-REVIEWED | Posted: 7 December 2023 doi:10.20944/preprints202312.0442.v1

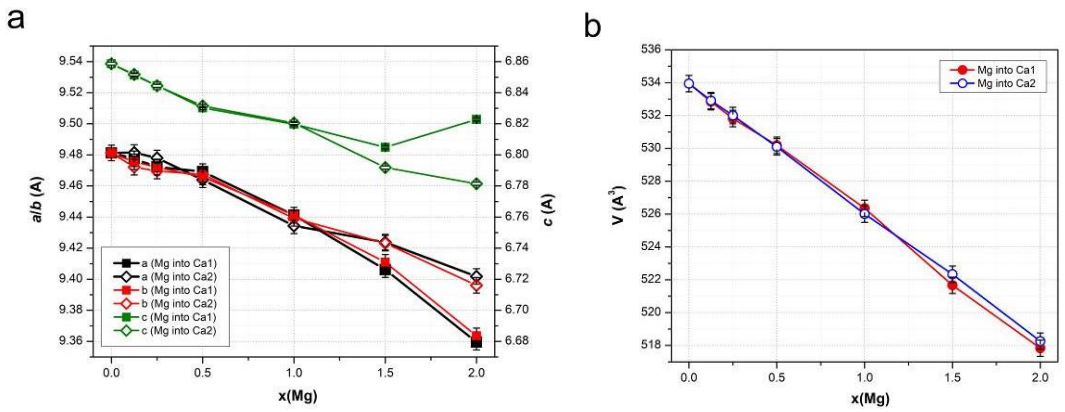

Figure 8. Changes in the parameters (**a**) and volumes (**b**) of the Mg-HA unit cell depending on the concentration *x* of magnesium cations in Ca1 and Ca2 positions. The results of DFT calculations for the substitution in a supercell consisting of 8 unit cells.

Comparison of the results of modeling (Figure 8) with the experimental data (Figure 4) suggests that during the synthesis of Mg-HA, the substitution of calcium by magnesium predominantly occurs in the Ca2 position. This is also indicated by the calculated values of the formation energy (E_f) of the substitutions of calcium for magnesium in the positions Ca1 and Ca2 shown in Figure 9.

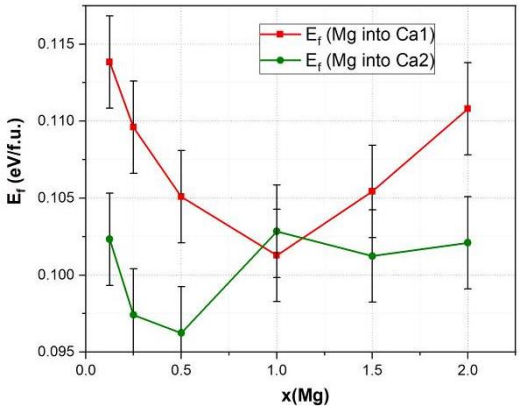

Figure 9. Formation energy E_f of calcium by magnesium substitutions in the supercell at the Ca1 and Ca2 positions as a function of the number of substituted *x* ions.

Figure 9 shows that the dependence of E_f on the magnesium concentration in Ca1 position has a parabolic shape with a minimum at $x = 1$. The E_f values for substitutions in Ca2 position change irregularly as the concentration *x* increases. As seen, all the values except for those at $x = 1$ are below the E_f values for substitutions in Ca1 position, i.e., $E_f(Ca1) > E_f(Ca2)$. At a concentration $x = 1$, the formation energy values for both Mg substitutions are close, which means that the magnesium cation can coexist at the positions Ca1 and Ca2.

From the above, we can conclude that for almost all values of *x*, Mg substitution in the Ca2 position is energetically more favorable than in the Ca1 position, hence, the substitution in the Ca2 position mainly occurs during Mg-HA synthesis.

3.3. Thermal Stability of Mg-HA

The thermal stability of the Mg-HA samples synthesized using $Mg(H_2PO_4)_2{\cdot}2H_2O$ was investigated. Figure 6 shows the changes in the XRD patterns of Mg-HA samples at different concentrations *x* of magnesium after heat treatment at different temperatures. As seen, the substituted samples are less stable than unsubstituted HA. Upon decomposition of Mg-HA, the reflections of β-TCP and MgO appear in the XRD patterns, which was also reported by Moreira et al. [44].

Preprints (www.preprints.org) | NOT PEER-REVIEWED | Posted: 7 December 2023 doi:10.20944/preprints202312.0442.v1

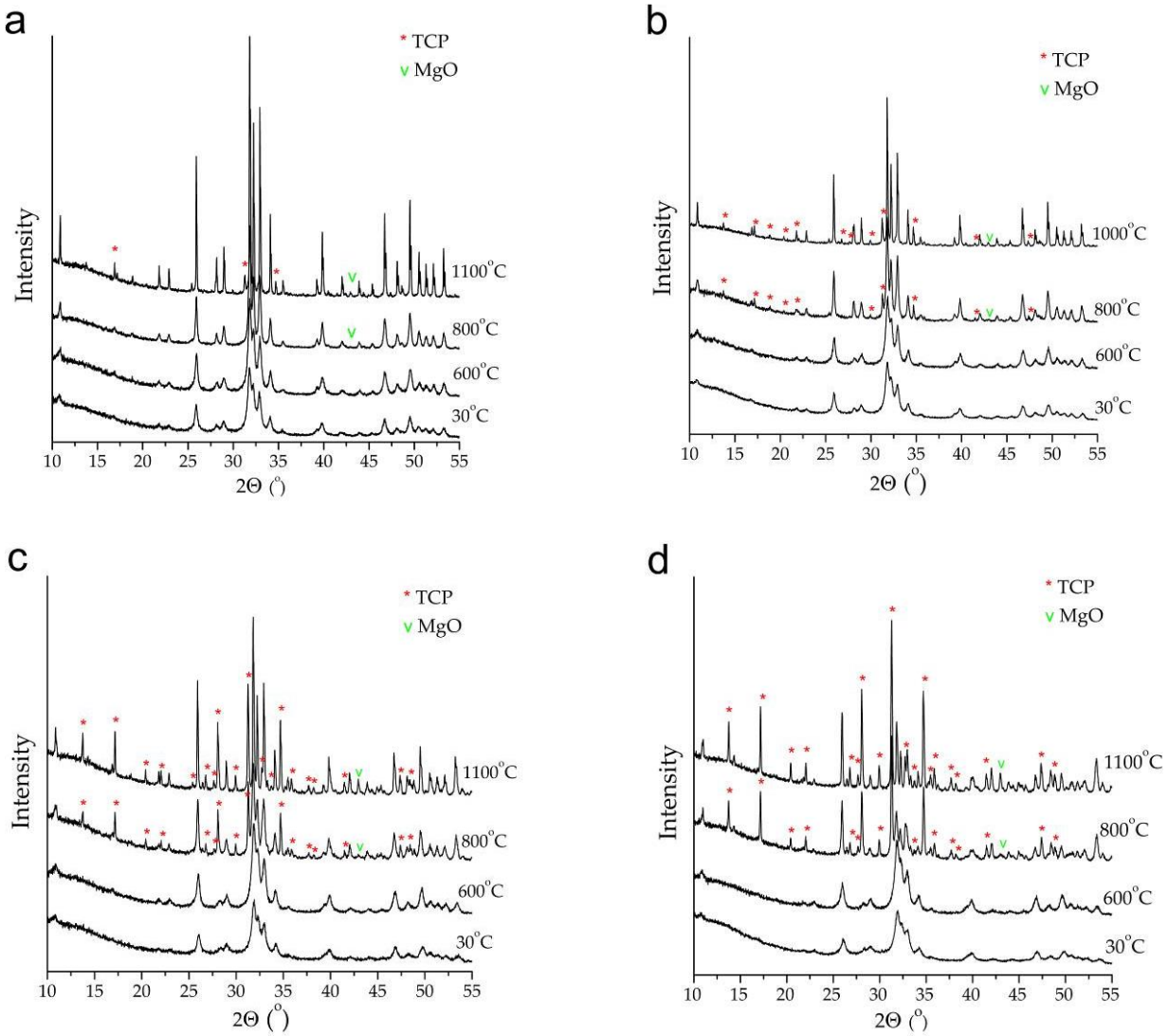

Figure 10. XRD patterns of the Mg-HA samples with magnesium concentration $x = 0.25$ (**a**), $x = 0.5$ (**b**), $x = 1.0$ (**c**), and $x = 2.0$ (**d**) after heat treatment at different temperatures. Unmarked reflections belong to the HA phase.

The results of the quantitative phase analysis of the XRD patterns by modeling their profiles showed that the decomposition of Mg-HA proceeds in two stages and the starting temperature of this process depends on the concentration of magnesium in the Mg-HA structure. As can be seen from Table 3, at a concentration $x = 0.25$, the sample remains single-phase up to 700 °C inclusive, whereas at 800 °C, a nanosized phase of magnesium oxide is formed. At higher values of x, the MgO phase appears already at 700 °C. A further increase in the temperature up to 800 °C results in the formation of the second impurity phase, β-TCP, whereas the concentration of MgO increases. The amounts of MgO and β-TCP increase as the magnesium concentration in Mg-HA increases.

Table 3. Phase composition (wt.%) of the Mg-HA samples with different magnesium (x) concentrations after heating at different temperatures.

x(Mg)	Phase	Temperature (°C)					
		600	700	800	900	1100	1200
0.25	HA	100	100	99.7	94.1	94.1	91.1
	MgO	–	–	0.3	0.5	0.8	0.6
	TCP	–	–	–	5.4	7.2	8.3

Preprints (www.preprints.org) | NOT PEER-REVIEWED | Posted: 7 December 2023 doi:10.20944/preprints202312.0442.v1

0.5	HA	100	99.9	88.8	81.1	80.7	79.6
	MgO	–	0.1	1.0	1.4	1.3	1.3
	TCP	–	–	10.2	17.5	17.9	19.0
1.0	HA	100	99.0	70.0	58.0	56.8	54.6
	MgO	–	1.0	2.0	2.6	2.6	2.8
	TCP	–	–	28.0	39.4	40.6	42.6
1.5	HA	100	96.6	36.2	27.6	28.0	25.7
	MgO	–	3.4	4.7	4.3	4.2	4.1
	TCP	–	–	59.1	68.1	67.8	70.2
2.0	HA	100	94.3	14.3	6.1	5.1	6.4
	MgO	–	3.1	6.6	5.9	5.7	5.8
	TCP	–	2.6	79.1	88.0	89.3	87.8

Figure 8a,b shows that, unlike the samples heated at 500 °C, the unit cell parameters and volume of the HA phase, annealed at 900 °C with the formation of the impurity phases MgO and β-TCP, almost do not change (Figure 8c,d) (Figure 5a-c). This implies that the HA structure after the formation of the impurity phases does not contain magnesium cations. At the same time, the unit cell parameter values of the β-TCP phase are a = 10.34 Å and c = 37.20 Å, which is much smaller than those reported by Bohner et al. [45]. Consequently, the β-TCP phase contains magnesium cations, which agrees with the data reported in studies [13, 32].

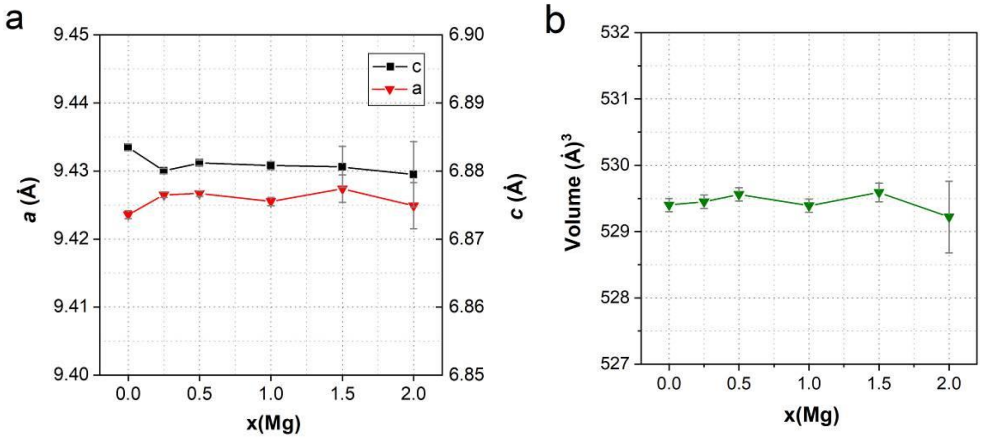

Figure 12. Variation of the parameters a and c (**a**), and unit cell volume (**b**) of the HA phase in the samples with different concentrations of the introduced magnesium after annealing at 900 °C.

Taking into account that the decomposition of Mg-HA proceeds in two stages with the formation of MgO in the first stage and the substituted β-TCP and MgO in the second stage, the decomposition of Mg-HA can be described by Reactions (6)–(7):

$$Ca_{10-x}Mg_x(PO_4)_6(OH)_2 \xrightarrow{t^\circ} Ca_{10-x}Mg_{x-y}(PO_4)_6(OH)_{2-2y} + yMgO + yH_2O, \quad (6)$$

where y ≤ 0.5

$$Ca_{10-x}Mg_{x-y}(PO_4)_6(OH)_{2-2y} \xrightarrow{t^\circ} (1-x)Ca_{10}(PO_4)_6(OH)_2 + 3xCa_{3-x+y+z}Mg_{x-y-z}(PO_4)_2 + zMgO + nH_2O, \quad (7)$$

At the first stage of the decomposition proceeding by Reaction (6), Mg-HA, which contains a small concentration of cationic vacancies and magnesium oxide, is formed. At the second stage of the decomposition proceeding by Reaction (7) at a slightly higher temperature, the number of hydroxyl groups in the apatite structure decreases to less than 1, so the crystal lattice of the substituted apatite becomes unstable and decomposes into the substituted β-TCP and MgO. Magnesium substitution for calcium cations in the structure of β-TCP was also reported in studies [21,23,32].

Preprints (www.preprints.org) | NOT PEER-REVIEWED | Posted: 7 December 2023 doi:10.20944/preprints202312.0442.v1

The significant difference between ionic radii of calcium and magnesium may be the reason for the decomposition of Mg-HA. In this case, the magnesium cations, which partially occupy the calcium positions, are located at a much larger distance from their nearest neighboring oxygen anions than the calcium cations in the same position. The thermal expansion of the crystal lattice upon heating resulting in a further increase in the ion-ion distances lead to the destruction of the ionic crystal at the sites of localization of the magnesium cations followed by the formation of β-TCP and MgO phases. It is noteworthy that, for all concentrations of the introduced magnesium, the behavior of the crystallite size of the substituted apatite phase after cooling and unsubstituted HA (Figure 7), which does not undergo any structural transformations in this temperature range, have the same dynamic. Even at x = 2, when the Mg-HA structure is almost completely decomposed (only 6 % HA remains), the changes in the crystallite sizes have the same dynamics. Consequently, the Mg-HA structure decomposes upon heating.

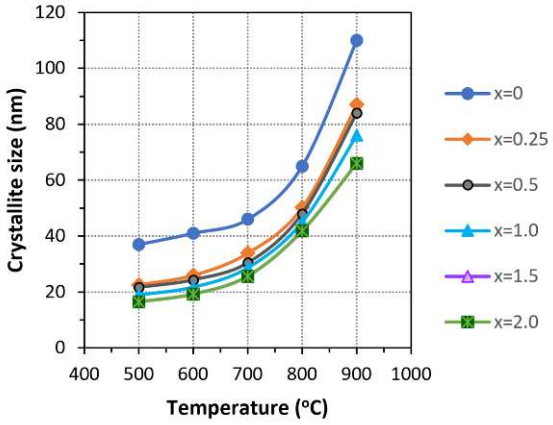

Figure 11. Evolution of the apatite crystallite size with temperature upon heating Mg-HA containing different magnesium concentrations.

4. Conclusions

Mg-substituted HA of the composition $Ca_{10-x}Mg_x(PO_4)_6(OH)_2$ was synthesized by the mechanochemical method. It was shown that magnesium hydroxide or monomagnesium phosphate should be used as the magnesium-bearing reagents. The interaction of these compounds with the other components of the reaction mixture (CaO and $CaHPO_4$) during mechanical treatment in a planetary ball mill results in the formation of a single-phase substituted apatite directly in the mill without further heat treatment. In the case of magnesium oxide, the reaction does not proceed entirely to completion; as a result, a non-stoichiometric, partially substituted apatite containing an impurity phase of the initial MgO, is formed.

Mg-substituted HA prepared by the mechanochemical synthesis contains lattice and adsorbed water in the amount of no more than 7.2 wt.%, which is removed upon heating at 500 °C. An increase in the Mg content introduced into HA leads to a decrease in the unit cell parameters, its volume, and the crystallite size as well. The results of DFT calculations performed on the HA supercell model of 352 atoms showed similar dynamics of the changes in the unit cell parameters. Moreover, it was found that, the dependence of cell parameters from the degree of substitution significantly deviated from linear behaviour at large values of *x* for magnesium substitution in the Ca1 position. A comparison of the experimental and the calculated cell parameters, suggests that, magnesium substitutions in both Ca1 and Ca2 positions can occur but the Ca2 position demonstrate the behavior closer the observed one under the conditions of mechanochemical synthesis. This result is also confirmed by the consideration of the calculated energies of formation of Mg substitutions in the Ca1 and Ca2 positions.

The study of thermal stability of the Mg-substituted HA has shown that the introduction of magnesium cations destabilizes the HA structure, thereby, upon heating of the samples above 600

°C, Mg-HA decomposes. The starting temperature of thermal decomposition depends on the concentration of magnesium in the sample. The more magnesium in the Mg-HA structure, the lower temperature at which decomposition starts. Thus, at a concentration x = 0.25, the samples remain single-phase up to a temperature of 700 °C, while at higher values of x, the decomposition starts at 700 °C. The decomposition of Mg-HA proceeds in 2 stages. At the first stage, the MgO phase is formed. A further increase in the temperature by 100 °C results in the formation of another impurity phase, β-TCP. The concentrations of the released MgO and β-TCP phases increase as the magnesium concentration in Mg-HA increases. After the release of magnesium oxide, the remaining HA phase does not contain magnesium cations in its lattice, while the phase of another phosphate, β-TCP, contains magnesium cations.

Supplementary Materials: No supplementary materials are available.

Author Contributions: Conceptualization, V.S.B. and N.V.B.; Funding acquisition, V.S.B.; Investigation, S.V.M., I.A.B., O.B.V., I.Y.P., N.V.E. and E.V.P.; Methodology, N.V.B. and V.S.B.; Resources, L.A.A., N.V.B. and V.S.B.; Software, S.V.M., N.V.E., N.V.B. and V.S.B.; Writing – original draft, N.V.B. and N.V.E.; Writing – review & editing, L.A.A., N.V.B., S.V.M., I.A.B., O.A.L. and V.S.B. All authors have read and agreed to the published version of the manuscript.

Funding: The study was supported by a grant Russian Science Foundation (RSF), No. 21-12-00251.

Institutional Review Board Statement: Not applicable.

Informed Consent Statement: Not applicable.

Data Availability Statement: The raw/processed data required to reproduce these results are included in the Materials and Methods section.

Acknowledgments: The authors thank Prosanov I.Yu. and Gerasimova K.B. for measuring IR spectra and performing thermal analysis, respectively.

Conflicts of Interest: The authors declare no conflict of interest.

References

1. Thirumalai, J. Hydroxyapatite: advances in composite nanomaterials, biomedical applications and its technological facets. Intech Open, London, **2018**. https://dx.doi.org/10.5772/intechopen.68820.
2. Dorozhkin, S.V. Calcium orthophospates ($CaPO_4$): occurrence and properties. *Prog. Biomater*., **2016**, *5*, 9–70. https://doi.org/10.1007/s40204-015-0045-z.
3. Ratner, B.D.; Hoffman, A.S.; Schoen, F.J.; Lemons, J.E. Biomaterials Science, 3rd ed.; Academic Press: Oxford, UK, **2013.** ISBN: 978-0-12-374626-9.
4. Elliott, J.C. Structure and chemistry of the apatites and other calcium orthophosphates; Elsevier Science: Amsterdam, The Netherlands, **1994**. ISBN: 0-444-81582-1.
5. Supova, M. Substituted hydroxyapatites for biomedical applications: A review. *Ceram. Int*., **2015**, *41*, 9203–9231. https://doi.org/10.1016/j.ceramint.2015.03.316.
6. Tite, T.; Popa, A.-C.; Balescu, L.M.; Bogdan, I.M.; Pasuk, I.; Ferreira, J.M.F.; Stan, G.E. Cationic substitutions in hydroxyapatite: current status of the derived biofunctional effects and their in vitro interrogation methods. *Materials*, **2018**, *11*, 2081. https://doi.org/10.3390/ma11112081.
7. Pepa, G. D.; Brandi, M. L. Microelements for bone boost: the last but not the least. Review. *Clin. Cases Miner. Bone Metab*.**, 2016**, *13*, 3, 181-185. doi: 10.11138/ccmbm/2016.13.3.181.
8. Lagier, R.; Baud, C.-A. Magnesium whitlockite, a calcium phosphate crystal of special interest in pathology. *Pathol. Res. Pract*., **2003**, *199*, 5, 329-335. https://doi.org/10.1078/0344-0338-00425.
9. Rude, R. K. Magnesium deficiency: a cause of heterogenous disease in humans. *J. Bone Miner. Res.*, **1998**, *13*, 4, 749-758. https://doi.org/10.1359/jbmr.1998.13.4.749.
10. Serre, C. M.; Papillard, M.; Chavassieux, P.; Voegel, J. C.; Boivin G. Influence of magnesium substitution on a collagen-apatite biomaterial on the production of a calcifying matrix by human osteoblasts. *J. Biomed. Mater.Res*. **1998**, *42*, 4, 626-633. doi: 10.1002/(sici)1097-4636(19981215)42:4<626::aid-jbm20>3.0.co;2-s.
11. Ergun, C.; Webster, T. J.; Bizias, R.; Doremus, R. H. Hydroxylapatite with substituted magnesium, zinc, cadmium, and yttrium. I. Structure and microstructure. *J. Biomed. Mater. Res.*, **2002**, *59*, 2, 305-311. doi: 10.1002/jbm.1246.
12. Creedon, A.; Flynm, A.; Cashman K. The effect of moderately and severely restricted dietary magnesium intakes on bone composition and bone metabolism in the rat. *British Journal of Nutrition*, **2007**, *82*, 1, 63-71. doi: 10.1017/S0007114599001130.

13. Kannan, S.; Lemos, I. A. F; Rocha, J. H. G; Ferreira, J. M. F. Synthesis and characterization of magnesium substituted biphasic mixtures of controlled hydroxyapatite/β-tricalcium phosphate ratios. *J. Sol. St. Chem*., **2005**, *178*, 10, 3190-3196. https://doi.org/10.1016/j.jssc.2005.08.003.
14. Rude, R. K.; Singer, F. R.; Gruber, H. E. Skeletal and hormonal effects of magnesium deficiency. *Journal of the American College of Nutrition*, **2009**, *28*, 2, 131-141. https://doi.org/10.1080/07315724.2009.10719764.
15. Toba, Y.; Kajita, Y.; Masuyama, R.; Takada, Y.; Suzuki, K.; Aoe, S. Dietary magnesium supplementation affects bone metabolism and dynamic strength of bone in ovariectomized rats. Journal of Nutrition, **2000**, *130*, 2, 216-220 https://doi.org/10.1093/jn/130.2.216.
16. Landi, E.; Logroscino, G.; Proietti, L; Tampieri, A.; Sandri, M.; Sprio, S. Biomimetic Mg-substituted hydroxyapatite: from synthesis to in vivo behavior. *J Mater Sci: Mater Med*., **2008**, *19*, 239–247. https://doi.org/10.1007/s10856-006-0032-y
17. Stipniece, L.; Salma-Ancane, K.; Borodajenko, N.; Sokolova, M.; Jakovlevs, D.; Berzina-Cimdina, L. Characterization of Mg-substituted hydroxyapatite synthesized by wet chemical method. *Ceram. Int*., **2014**, *40*, 2, 3261-3267. https://doi.org/10.1016/j.ceramint.2013.09.110.
18. Suchanek, W. L.; Byrappa, K.; Shuk, P.; Riman, R. E.; Janas, V. F. Kevor; TenHuisen, S. Preparation of magnesium-substituted hydroxyapatite powders by the mechanochemical–hydrothermal method. *Biomaterials*, **2004**, *25*, 19, 4647-4657. https://doi.org/10.1016/j.biomaterials.2003.12.008.
19. Ren, F.; Leng, Y.; Xin, R.; Ge, X. Synthesis, characterization and ab initio simulation of magnesium-substituted hydroxyapatite. *Acta Biomater*., **2010**, 6, 2787–2796. https://doi.org/10.1016/j.actbio.2009.12.044
20. Goldberg, M. A.; Fomin, A. S.; Murzakhanov, F. F.; Makshakova, O. N.; Donskaya, N. O.; Antonova, O. S.; Gnezdilov, O. I.; Mikheev, I. V.; Knotko, A. V.; Kudryavtsev, E. A.; Akhmedova, S. A.; Sviridova, I. K.; Sergeeva, N. S.; Mamin, G. V.; Barinov, S. M.; Gafurov, M. R.; Komlev, V. S. The improved textural properties, thermal stability, and cytocompatibility of mesoporous hydroxyapatite by Mg2+ doping. *Materials Chemistry and Physics*, **2022**, *289*, 126461. https://doi.org/10.1016/j.matchemphys.2022.126461.
21. Nagyné-Kovács, T.; Studnicka, L.; Kincses, A.; Spengler, G.; Molnár, M.; Tolner, M.; Lukács, I. E.; Szilágyi, I. M.; Pokol, G. Synthesis and characterization of Sr and Mg-doped hydroxyapatite by a simple precipitation method. *Ceram. Int*., **2018**, *44*, 18, 22976-22982. https://doi.org/10.1016/j.ceramint.2018.09.096.
22. Farzadi, A.; Bakhshi, F.; Solati-Hashjin, M.; Asadi-Eydivand, M.; A. abu Osman, N. Magnesium incorporated hydroxyapatite: Synthesis and structural properties characterization. *Ceram. Int*., **2014**, *40*, 4, 6021-6029. https://doi.org/10.1016/j.ceramint.2013.11.051.
23. Mayer, I.; Schlam, R.; Featherstone, J.D.B. Magnesium-containing carbonate apatites, *J. Inorg. Biochem*., **1997**, *66*, 1, 1-6. https://doi.org/10.1016/S0162-0134(96)00145-6.
24. Cox, S. C.; Jamshidi, P.; Grover, L. M.; Mallick, Kajal K. Preparation and characterisation of nanophase Sr, Mg, and Zn substituted hydroxyapatite by aqueous precipitation. *Materials Science and Engineering: C*, **2014**, *35*, 106-114. https://doi.org/10.1016/j.msec.2013.10.015.
25. Yasukawa, A.; Ouchi, S.; Kandori, K.; Ishikawa, T. Preparation and characterization of magnesium–calcium hydroxyapatites. J. Mater. Chem., **1996**, *6*, 8, 1401–1405. doi:10.1039/jm9960601401.
26. Shepherd, J.H.; Shepherd, D.V.; Best, S.M. Substituted hydroxyapatites for bone repair. *J Mater Sci: Mater Med*., **2012**, *23*, 2335–2347. https://doi.org/10.1007/s10856-012-4598-2.
27. Geng, Z.; Cui, Z.; Li, Z.; Zhu, S. Liang, Y.; Lu, W. W.; Yang X. Synthesis, characterization and the formation mechanism of magnesium- and strontium-substituted hydroxyapatite. *J. Mater. Chem. B*., **2015,** *3*, 3738-3746. DOI: 10.1039/c4tb02148g.
28. Moussa, S. B.; Mehri, A.; Gruselle, M.; Beaunier, P., Costentin, G.; Badraoui, B. Combined effect of magnesium and amino glutamic acid on the structure of hydroxyapatite prepared by hydrothermal method. *Materials Chemistry and Physics*, **2018**, *212*, 21–29. doi:10.1016/j.matchemphys.2018.03.017.
29. Evis, Z.; Sun. Z. P. Structural and mechanical investigations of magnesium and fluoride doped nanosize calcium phosphates. *Journal of Ceramic Processing Research*, **2010**, *11*, 6, 701-715.
30. Bigi, A.; Foresti, E.; Gregorini, R.; Ripamonti, A.; Roveri, N.; Shah. J.S. The role of magnesium on the structure of biological apatites. *Calcif Tissue Int*., **1992**, *50*, 5, 439-44. doi: 10.1007/BF00296775.
31. Bertoni, E.; Bigi, A.; Cojazzi, G.; Gandolfi, M.; Panzavolta, S.;, Roveri, N. Nanocrystals of magnesium and fluoride substituted hydroxyapatite. *J Inorg Biochem*., **1998**, *72*, 1-2, 29-35. doi: 10.1016/s0162-0134(98)10058-2.
32. Gomes, S.; Renaudin, G.; Jallot, E.; Nedelec, J.M. Structural characterization and biological fluid interaction of Sol-Gel-derived Mg-substituted biphasic calcium phosphate ceramics. *ACS Appl Mater Interfaces*, **2009**, *1*, 2, 505-13. doi: 10.1021/am800162a.
33. Ezhova, Zh. A.; Koval, E. M.; Orlovskii, V. P. Synthesis and physicochemical study of collagen-containing calcium carbonatehydroxyapatites. *Rus. J. Inorg. Chem*., **2003**, 48, 2, 284-287. https://elibrary.ru/item.asp?id=13424936
34. Rietveld, H.M. A Profile Refinement Method for Nuclear and Magnetic Structures. *J. Appl. Cryst*. **1969**, *2*, 65–70. https://doi.org/10.1107/S0021889869006558.

35. Bystrov, V. S.; Paramonova, E. V.; Avakyan, L. A.; Eremina, N. V.; Makarova, S. V.; Bulina, N. V. Effect of Magnesium Substitution on Structural Features and Properties of Hydroxyapatite. *Materials*, **2023**, *16*, 17, 5945. https://doi.org/10.3390/ma16175945.
36. Heyd, J.; Scuseria, G. E.; Ernzerhof, M. Hybrid functionals based on a screened Coulomb potential. *J. chem. phys*., **2003**, *118*, 18, 8207-8215. https://doi.org/10.1063/1.1564060.
37. Krukau, A. V.; Vydrov, O. A.; Izmaylov, A. F.; Scuseria, G. E. Influence of the exchange screening parameter on the performance of screened hybrid functionals. *J. chem. Phys*., **2006**, *125*, 22, 224106. https://doi.org/10.1063/1.2404663.
38. Perdew, J.P.; Burke, K.; Ernzerhof, M. Generalized gradient approximation made simple. *Phys. Rev. Lett*., **1996**, *77*, 3865–3868. https://doi.org/10.1103/PhysRevLett.77.3865.
39. Quantum ESPRESSO. Available online: https://www.quantum-espresso.org/ (accessed on 27 October 2023)
40. Aryal, S.; Matsunaga, K.; Ching, W.Y. Ab initio simulation of elastic and mechanical properties of Zn- and Mg-doped hydroxyapatite (HAP). *J. Mech. Behav. Biomed. Mater*. **2015**, 47, 135–146. https://doi.org/10.1016/j.jmbbm.2015.03.018.
41. Shannon, R.D. Revised effective ionic radii and systematic studies of interatomic distances in halides and chalcogenides. *Acta cryst. A.* ***1976***, *32,* 5, 751–767. https://doi.org/10.1107/S0567739476001551.
42. Chaikina, M.V.; Bulinaa, N.V.; Vinokurova, O.B.; Prosanov, I.Y.; Dudina, D.V. Interaction of calcium phosphates with calcium oxide or calcium hydroxide during the "soft" mechanochemical synthesis of hydroxyapatite. *Ceram. Int.* **2019**, *45*, 16927–1693. https://doi.org/10.1016/j.ceramint.2019.05.239.
43. Chaikina, M.V.; Bulina, N.V.; Vinokurova, O.B.; Gerasimov, K.B.; Prosanov, I.Y.; Kompankov, N.B.; Lapina, O.B.; Papulovskiy, E.S.; Ischenko, A.V.; Makarova, S.V. Possibilities of mechanochemical synthesis of apatites with different Ca/P ratios. *Ceramics* **2022**, *5*, 404–422. https://doi.org/10.3390/ceramics5030031.
44. Moreira, M.P.; de Almeida Soares, G.D.; Dentzer, J.; Anselme, K.; de Sena, L.Á.; Kuznetsov, A.; dos Santos, E.A. Synthesis of magnesium- and manganese-doped hydroxyapatite structures assisted by the simultaneous incorporation of strontium. *Mater Sci Eng C Mater Biol Appl*. **2016**, 1, 61, 736-43. doi: 10.1016/j.msec.2016.01.004
45. Bohner, M.; Santoni, L.B.G.; Döbelin, N. β-tricalcium phosphate for bone substitution: Synthesis and properties. *Acta Biomater.* **2020**, *113*, 23–41. https://doi.org/10.1016/j.actbio.2020.06.022.